Important Notice to Authors

No further publication processing will occur until we receive your response to this proof.

Attached is a PDF proof of your forthcoming article in PRA. Your article has 11 pages and the Accession Code is **AQ12222**.

Please note that as part of the production process, APS converts all articles, regardless of their original source, into standardized XML that in turn is used to create the PDF and online versions of the article as well as to populate third-party systems such as Portico, Crossref, and Web of Science. We share our authors' high expectations for the fidelity of the conversion into XML and for the accuracy and appearance of the final, formatted PDF. This process works exceptionally well for the vast majority of articles; however, please check carefully all key elements of your PDF proof, particularly any equations or tables.

Figures submitted electronically as separate files containing color appear in color in the online journal. However, all figures will appear as grayscale images in the print journal unless the color figure charges have been paid in advance, in accordance with our policy for color in print (https://journals.aps.org/authors/color-figures-print).

Specific Questions and Comments to Address for This Paper

1 Please provide city and zip code for affiliation 2 and 3.
2 Please see **http://publish.aps.org/authors/new-novel-policy-physical-review** for Phys. Rev. policy on new/novel phrases.
3 Please check changes to "bowtie- shaped" and "diamond-shaped".
4 Please check insertions of "Grant".
5 Please check all information in Ref. [4].
FQ: This funding provider could not be uniquely identified during our search of the FundRef registry (or no Contract or Grant number was detected). Please check information and amend if incomplete or incorrect.

ORCIDs: Please follow any ORCID links (iD) after the authors' names and verify that they point to the appropriate record for each author. Requests to add ORCIDs should be sent no later than the first proof revisions. See complete details regarding ORCID requests and ORCID verification at https://journals.aps.org/authors/adding-orcids-during-proof-corrections.
NOTE: If this paper is an Erratum or a Reply, the corresponding author's ORCID may be present if previously provided to APS, but no ORCIDs can be added at proof stage.

Crossref Funder Registry ID: Information about an article's funding sources is now submitted to Crossref to help you comply with current or future funding agency mandates. Crossref's Funder Registry (https://www.crossref.org/services/funder-registry/) is the definitive registry of funding agencies. Please ensure that your acknowledgments include all sources of funding for your article following any requirements of your funding sources. Where possible, please include grant and award ids. Please carefully check the following funder information we have already extracted from your article and ensure its accuracy and completeness:
National Natural Science Foundation of China, 12074061, 11861131001
Italian Ministry of Foreign Affairs and International Cooperation, PGR00960
National Key Research and Development Program of China, 2021YFE0193500
Scientific and Technological Research Program of Jilin Education Department, JJKH20211280KJ

Other Items to Check

- Please note that the original manuscript has been converted to XML prior to the creation of the PDF proof, as described above. Please carefully check all key elements of the paper, particularly the equations and tabular data.
- Title: Please check; be mindful that the title may have been changed during the peer-review process.
- Author list: Please make sure all authors are presented, in the appropriate order, and that all names are spelled correctly.
- Please make sure you have inserted a byline footnote containing the email address for the corresponding author, if desired. Please note that this is not inserted automatically by this journal.
- Affiliations: Please check to be sure the institution names are spelled correctly and attributed to the appropriate author(s).
- Receipt date: Please confirm accuracy.
- Acknowledgments: Please be sure to appropriately acknowledge all funding sources.
- Hyphenation: Please note hyphens may have been inserted in word pairs that function as adjectives when they occur before a noun, as in "x-ray diffraction," "4-mm-long gas cell," and "*R*-matrix theory." However, hyphens are deleted from word pairs when they are not used as adjectives before nouns, as in "emission by x rays," "was 4 mm in length," and "the *R* matrix is tested."

  Note also that Physical Review follows U.S. English guidelines in that hyphens are not used after prefixes or before suffixes: superresolution, quasiequilibrium, nanoprecipitates, resonancelike, clockwise.

- Please check that your figures are accurate and sized properly. Make sure all labeling is sufficiently legible. Figure quality in this proof is representative of the quality to be used in the online journal. To achieve manageable file size for online delivery, some compression and downsampling of figures may have occurred. Fine details may have become somewhat fuzzy, especially in color figures. The print journal uses files of higher resolution and therefore details may be sharper in print. Figures to be published in color online will appear in color on these proofs if viewed on a color monitor or printed on a color printer.
- Please check to ensure that reference titles are given as appropriate.
- Overall, please proofread the entire *formatted* article very carefully. The redlined PDF should be used as a guide to see changes that were made during copyediting. However, note that some changes to math and/or layout may not be indicated.

Ways to Respond

- ***Web:*** If you accessed this proof online, follow the instructions on the web page to submit corrections.
- ***Email:*** Send corrections to praproofs@aptaracorp.com
  Subject: **AQ12222** proof corrections
- ***Fax:*** Return this proof with corrections to +1.703.791.1217. Write **Attention:** PRA Project Manager and the Article ID, **AQ12222**, on the proof copy unless it is already printed on your proof printout.

PHYSICAL REVIEW A **00**, 003700 (2022)

Photon-pair generation on resonance via a dark state

Hui-Min Zhao,[1] Xiao-Jun Zhang,[1,*] M. Artoni,[2,3,†] G. C. La Rocca,[4] and Jin-Hui Wu[1,‡]

[1]*School of Physics, Northeast Normal University, Changchun 130024, China*
[2]*Department of Chemistry and Physics of Materials, University of Brescia, Italy*
[3]*European Laboratory for Non-Linear Spectroscopy, Sesto Fiorentino, Italy*
[4]*NEST, Scuola Normale Superiore, Piazza dei Cavalieri 7, I-56126 Pisa, Italy*

(Received 14 March 2022; revised 26 June 2022; accepted 3 August 2022; published xxxxxxxxxx)

We present a scheme to generate photon-pair states through resonant spontaneous four-wave mixing (SFWM) in a five-level double-bowtie ($\triangleright\!\triangleleft$) configuration subject to two pumping fields and one coupling field when a *quasidark state* is created between two of three ground levels. The quasidark state is used here to largely suppress linear resonant absorption (gain) of the generated photon pairs while supporting strong SFWM nonlinearities and nonclassical cross-correlation. Numerical results for cold atomic samples show that the generation efficiency may be comparable to or even larger than that obtained in the more familiar off-resonance four-level single-bowtie configuration with only one pumping field. This scheme is robust to fluctuations of atomic populations and enables one to easily control the ratio of two rates with which distinct SFWM processes generate photon-pair states.

DOI: 10.1103/PhysRevA.00.003700

I. INTRODUCTION

Free of collisions and decoherence, flying photons are excellent carriers of information and natural qubits in long distance quantum communications [1]. Particularly, photon pairs, or biphotons, as a pair of single photons generated simultaneously provide us a practical route to overcome the probabilistic emission of typical photon sources by using one photon as a messenger to herald the other one, a qubit that needed to be operated. Besides being inherently time-energy entangled [2], photon pairs can be further constructed to produce other types of bipartite entanglement, e.g., in polarization [3], position-momentum [4], and even multiple degrees of freedom [5–9]. These advantages make the generation and manipulation of photon pairs become fundamental to the development of quantum science and technology such as quantum communications [10,11], cryptography [12], computation [13,14], teleportation [15], etc.

Photon pairs (*biphotons*) can be generated via spontaneous parametric down-conversion (SPDC) processes [16,17], yet these kind of biphotons are not appropriate for long distance quantum communications due to negative characteristics such as large bandwidths and short coherence times [18]. Biphotons generated from spontaneous four-wave mixing (SFWM) processes [19], on the other hand, typically own small bandwidths of the order of atomic natural linewidths [20]. With such apparent advantages, biphotons generation and manipulation exploiting SFWM processes have been intensively studied in cold atoms [21–23] and hot vapors [24–26]. Relevant driving schemes include four-level double-Λ systems [i.e., bowtie-shaped ($\triangleright\!\triangleleft$) systems] [22] and double-ladder systems [i.e., diamond-shaped ($\Diamond$) systems] [27–29]. Normally, biphotons generated in a $\triangleright\!\triangleleft$-shaped system have narrower linewidths ($\sim$1 MHz), than those generated in a $\Diamond$-shaped system ($\sim$10 MHz) [20], because the latter works in a manner similar to SPDC.

Efficient generation of a pair of Stokes and anti-Stokes photons in the $\triangleright\!\triangleleft$-shaped systems usually requires a far-detuned moderate pumping field or a near resonant weak pumping field, in addition to a resonant strong coupling field, so as to guarantee that most atomic population remains in a ground level. Linear absorption from the most populated ground level can be well suppressed due to quantum interference in the regime of electromagnetically induced transparency (EIT) [30], while linear absorption (gain) from other roughly empty ground or excited levels is naturally negligible with little possibility of spontaneous decay [24,31–33]. Recent advances on SFWM in various extended $\triangleright\!\triangleleft$-shaped systems include the generation of Einstein-Podolsky-Rosen entanglement [2], hyperentangled photons [5], bright narrowband biphotons [32] and color-entangled photons [34,35], just to name a few. Efficient SFWM is usually impractical to be achieved in the exact resonant pumping regime where linear absorption (gain) tends to dominate nonlinear interactions.

Here we employ an alternative five-level double-bowtie scheme where two partially overlapping SFWM processes can be simultaneously attained while suppressing linear absorption and gain via coherent population trapping [36]. One main advantage of this scheme is that all driving fields can be taken on exact resonance, with most atoms trapped in a "quasi" dark state [37] comprising a superposition of two ground levels, each of which takes part in one or the other SFWM process. Note that many dark-state based schemes

*zhangxj037@nenu.edu.cn
†artoni@lens.unifi.it
‡jhwu@nenu.edu.cn

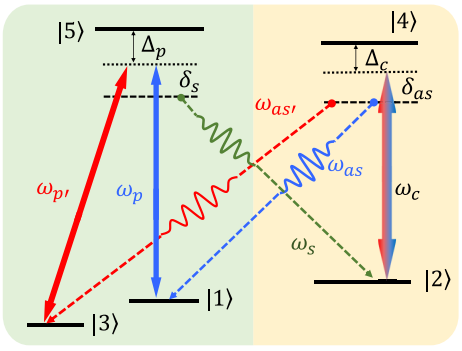

FIG. 1. Schematic diagram of a five-level double-$\triangleright\!\!\triangleleft$ configuration where a pumping ω_p ($\omega_{p'}$) and a coupling ω_c field are applied to generate a Stokes ω_s and an anti-Stokes ω_{as} ($\omega_{as'}$) photon via a SFWM process starting from the ground level $|1\rangle$ ($|3\rangle$). Under certain conditions this double-$\triangleright\!\!\triangleleft$-shaped system may be envisaged as the combination of a Λ subsystem driven by two pumping fields and a two-level subsystem driven by one coupling field. A quasidark state trapping most populations can be attained in the Λ subsystem enabling the generation of Stokes and anti-Stokes photon pairs even at exact resonance. The D_1 line of laser-cooled ^{87}Rb atoms is chosen here with levels $|1\rangle = |5S_{1/2}, F = 1, m = -1\rangle$, $|2\rangle = |5S_{1/2}, F = 2, m = 1\rangle$, $|3\rangle = |5S_{1/2}, F = 1, m = 1\rangle$, $|4\rangle = |5P_{1/2}, F = 1, m = 0\rangle$, and $|5\rangle = |5S_{1/2}, F = 2, m = 0\rangle$ as an example.

have appeared in different research fields for, e.g., realizing laser cooling [38,39], constructing conservative optical potentials [40,41], implementing Rydberg quantum gates [42], etc. Our detailed calculations on the linear and nonlinear susceptibilities reveal that destructive interference due to the dark state and negligible populations out of the dark state, caused by two resonant pumping fields of appropriate intensities, largely reduce linear absorption and gain, hence making our resonantly driven double-$\triangleright\!\!\triangleleft$-shaped system quite efficient in generating the Stokes and anti-Stokes photon pairs with very strong nonclassical cross-correlations.

The paper is organized as follows. In Sec. II, we introduce our five-level double-$\triangleright\!\!\triangleleft$-shaped system and discuss the quasidark state created by two resonant pumping fields. Section III is devoted to the suppressed absorption or gain properties of the Stokes and anti-Stokes fields described by the linear susceptibilities. In Sec. IV, we examine the nonclassical generation of the Stokes and anti-Stokes photon pairs arising from the enhanced nonlinear susceptibilities. Section V presents the quantitative comparison of our (resonant) double-$\triangleright\!\!\triangleleft$-shaped system to the (off-resonance) single-$\triangleright\!\!\triangleleft$-shaped system. Finally, we draw our conclusions in Sec. VI, while we give detailed calculations on the linear and nonlinear susceptibilities in the Appendix.

II. MODEL AND DARK STATE

We start by considering in Fig. 1 a five-level system where two pumping fields (ω_p, $\omega_{p'}$) and a coupling field (ω_c) are applied to drive atomic transitions $|1\rangle \leftrightarrow |5\rangle$, $|3\rangle \leftrightarrow |5\rangle$, and $|2\rangle \leftrightarrow |4\rangle$, respectively, with detunings $\Delta_p = \omega_{51} - \omega_p$, $\Delta_{p'} = \omega_{53} - \omega_{p'}$, and $\Delta_c = \omega_{42} - \omega_c$. We will restrict ourselves in the following to the specific case in which $\Delta_p = \Delta_{p'}$, whereby the Stokes and anti-Stokes photons will be generated in pairs through two *partially overlapping* SFWM processes $|1\rangle \to |5\rangle \to |2\rangle \to |4\rangle \to |1\rangle$ (A) and $|3\rangle \to |5\rangle \to |2\rangle \to |4\rangle \to |3\rangle$ (B). Specifically, one pair of Stokes (ω_s) and anti-Stokes (ω_{as}) photons will be generated with detunings $\Delta_s = \omega_{52} - \omega_s$ and $\Delta_{as} = \omega_{41} - \omega_{as}$ upon the destruction of one pair of pumping (ω_p) and coupling (ω_c) photons. Likewise, another pair of Stokes (ω_s) and anti-Stokes ($\omega_{as'}$) photons with detunings Δ_s and $\Delta_{as'} = \omega_{43} - \omega_{as'}$ will be generated upon the destruction of another pair of pumping ($\omega_{p'}$) and coupling (ω_c) photons. Conservation of energy enforces as usual that the two-photon detunings $\delta_s = \Delta_p - \Delta_s$ and $\delta_{as} = \Delta_c - \Delta_{as}$ cancel out ($\delta_s + \delta_{as} = 0$) in process A while $\delta_{s'} = \Delta_{p'} - \Delta_s$ and $\delta_{as'} = \Delta_c - \Delta_{as'}$ cancel out ($\delta_s + \delta_{as'} = 0$) in process B. For the specific case examined here ($\Delta_p = \Delta_{p'}$), it is convenient to further adopt the common two-photon detuning

$$\delta = \delta_s = \delta_{s'} = -\delta_{as} = -\delta_{as'}$$

as a frequency scale parameter.

The *full* dynamics of this five-level system is governed by a set of coupled equations for 25 density matrix elements ρ_{mn} with $m, n \in \{1, 2, 3, 4, 5\}$ referring to atomic population ($m = n$) or coherence ($m \neq n$) [37]. In addition to coherent evolution driven by the applied and generated fields, atoms are subject to spontaneous emission and coherence decay occurring, respectively, with rates Γ_{mn} and γ_{mn} for $m \neq n$. The two rates are related through $\gamma_{mn} = \sum_l (\Gamma_{ml} + \Gamma_{nl})/2$ with $l \neq m \neq n$ referring to all possible levels even out of our five-level system, and can be phenomenally included into the density matrix equations mentioned above. Using a perturbation method with respect to the generated Stokes and anti-Stokes fields, it is viable to attain the zeroth- and first-order solutions of ρ_{mn}. The zeroth-order ones correspond to the case with neither Stokes nor anti-Stokes fields, whereby our five-level system can be regarded as a combination of the Λ subsystem involving levels $\{|1\rangle, |3\rangle, |5\rangle\}$ and the two-level subsystem involving levels $\{|2\rangle, |4\rangle\}$. The two subsystems are not independent but connected by the cross decay rates Γ_{41}, Γ_{43}, and Γ_{52} as they are driven by two pumping fields of Rabi frequencies $\Omega_p^+ = \mu_{15}E_p^+/2\hbar$ and $\Omega_{p'}^+ = \mu_{35}E_{p'}^+/2\hbar$ and a coupling field of Rabi frequency $\Omega_c^+ = \mu_{24}E_c^+/2\hbar$, respectively, with μ_{mn} being relevant dipole moments. Here and in what follows, we take superscript "+" ("−") to denote the positive (negative) frequency component of each electric field, and will assume $\Omega_j = \Omega_j^+ = \Omega_j^-$ with $j \in \{p, p', c\}$ for simplicity though $\Omega_j^- = (\Omega_j^+)^*$ in general.

With identical pumping detunings $\Delta_p = \Delta_{p'}$, all atoms are expected to be trapped in a so-called (coherent) dark state $|D\rangle = (\Omega_{p'}|1\rangle - \Omega_p|3\rangle)/(\Omega_p^2 + \Omega_{p'}^2)^{1/2}$ in the ideal case referring to $\gamma_{31} \to 0$ [43–46]. Further considering balanced pumping Rabi frequencies $\Omega_p = \Omega_{p'}$, the dark state turns out to be $|D\rangle = (|1\rangle - |3\rangle)/\sqrt{2}$, yielding thus $\rho_{11} = \rho_{33} = -\rho_{13} = 1/2$. In reality, however, atomic collisions and laser linewidths will contribute to a finite decoherence rate $\gamma_{31} \neq 0$ such that the dark state becomes quasidark, leaving a small part of populations free of coherent trapping. Relevant zeroth-

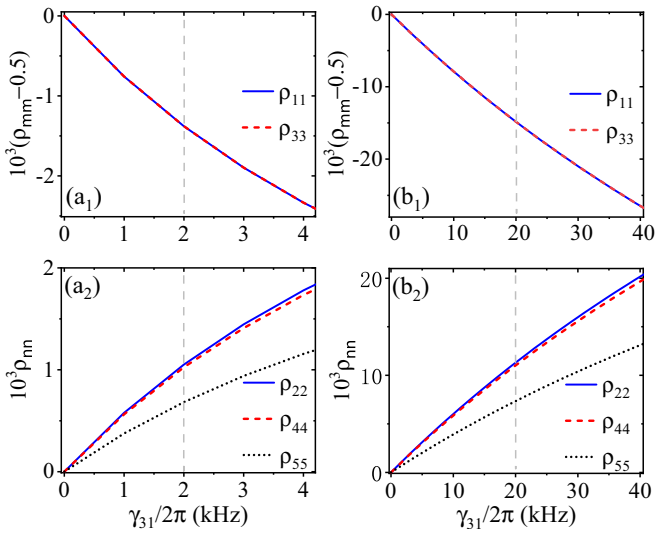

FIG. 2. Populations in the dark state (a_1),(b_1) and out of the dark state (a_2),(b_2) plotted against the ground-level decoherence rate γ_{31} with $\Gamma_{52,42} = 3\Gamma_{53,51,43,41} = \gamma/2$ and $\gamma_{54}/2 = \gamma_{53,52,51} = \gamma_{43,42,41} = \gamma$ by taking $\gamma \simeq 2\pi \times 3.0$ MHz and $\gamma_{32} = \gamma_{31} = \gamma_{21} = \gamma_0 \ll \gamma$ on the D_1 line of cold ^{87}Rb atoms. The pumping and coupling fields are applied with $\Delta_c = 0$, $\Delta_p = \Delta_{p'} = 0$, $\Omega_c = 4\gamma$, and $\Omega_p = \Omega_{p'} = \gamma/25$ in (a_1) and (a_2) while $\Omega_p = \Omega_{p'} = \gamma/5$ in (b_1) and (b_2).

order solutions are lengthy in general but become relatively simple,

$$\rho_{11}^{\langle 0\rangle} \simeq \rho_{33}^{\langle 0\rangle} \simeq \frac{1}{2}\big[1 - \rho_{22}^{\langle 0\rangle} - \rho_{44}^{\langle 0\rangle} - \rho_{55}^{\langle 0\rangle}\big], \tag{1a}$$

$$\rho_{22}^{\langle 0\rangle} \simeq \rho_{44}^{\langle 0\rangle} \simeq \frac{\Gamma_{52}}{\Gamma_{41}+\Gamma_{43}}\rho_{55}^{\langle 0\rangle} \simeq \frac{\Gamma_{52}}{P}\gamma_{31} \times\left[1 - \frac{\gamma_{31}(3\Gamma_{41}+3\Gamma_{43}+2\Gamma_{52})}{P} - \frac{\gamma_{31}\gamma_{51}}{2\Omega_p^2}\right], \tag{1b}$$

with $P = (\Gamma_{41}+\Gamma_{43})(\Gamma_{51}+\Gamma_{52}+\Gamma_{53})$, for resonant ($\Delta_p = \Delta_{p'} = \Delta_c = 0$) pumping and coupling fields restricted by $\Omega_c \gg \Gamma_{42}$ and $\Omega_p^2 = \Omega_{p'}^2 \gg \gamma_{31}\gamma_{51}/2$. It is clear that populations in the dark state $\rho_{11}^{\langle 0\rangle} + \rho_{33}^{\langle 0\rangle}$ may deviate more or less from unity and depend critically on a small ground-level decoherence rate γ_{31}. It is also important to stress that populations out of the dark state $\rho_{22}^{\langle 0\rangle} + \rho_{44}^{\langle 0\rangle} + \rho_{55}^{\langle 0\rangle}$ should not be too small in order to achieve efficient SFWM processes and meantime not too large in order to suppress linear absorption and gain as discussed below. Numerical calculations shown in Fig. 2 well support the above analytical results, i.e., a "quasi" dark state with $\rho_{22} \simeq \rho_{44} \simeq 1.5\rho_{55} \propto \gamma_{31}$ can be attained when γ_{31} is small enough, though deviations will become more and more evident (not shown) when γ_{31} increases to surpass, e.g., the vertical gray-dashed lines.

III. LINEAR ABSORPTION AND GAIN

First-order perturbative solutions for the atomic coherences $\rho_{52}^{\langle 1\rangle}$, $\rho_{41}^{\langle 1\rangle}$, and $\rho_{43}^{\langle 1\rangle}$ can be further attained which are directly related to the absorption (gain) and dispersion of Stokes and anti-Stokes photons generated in pairs $\{\omega_s, \omega_{as}\}$ and $\{\omega_s, \omega_{as'}\}$. With these solutions, it is easy to write down the corresponding induced polarizations $\hat{P}_{mn} = N_0\mu_{nm}\rho_{mn}^{\langle 1\rangle}$ for a sample of density N_0,

$$\hat{P}_{52}/\epsilon_0 = \chi_s^{(1)}\hat{E}_s^+ + \underbrace{\chi_{s,as}^{(3)}E_p^+E_c^+\hat{E}_{as}^-}_{\text{Proc. A}} + \underbrace{\chi_{s,as'}^{(3)}E_{p'}^+E_c^+\hat{E}_{as'}^-}_{\text{Proc. B}}, \tag{2a}$$

$$\hat{P}_{41}/\epsilon_0 = \chi_{as}^{(1)}\hat{E}_{as}^+ + \underbrace{\chi_{as,s}^{(3)}E_p^+E_c^+\hat{E}_s^-}_{\text{Proc. A}} + \underbrace{\chi_{as,as'}^{(3)}E_p^+E_{p'}^-\hat{E}_{as'}^+}_{\text{Proc. C}}, \tag{2b}$$

$$\hat{P}_{43}/\epsilon_0 = \chi_{as'}^{(1)}\hat{E}_{as'}^+ + \underbrace{\chi_{as',s}^{(3)}E_{p'}^+E_c^+\hat{E}_s^-}_{\text{Proc. B}} + \underbrace{\chi_{as',as}^{(3)}E_p^-E_{p'}^+\hat{E}_{as}^+}_{\text{Proc. C}}. \tag{2c}$$

Here electric fields for the applied fields have been taken as *classical* quantities, while those for the generated fields are assumed to be *quantum* described by operators

$$\hat{E}_j^+ = \frac{1}{\sqrt{2\pi}}\int d\omega_j\sqrt{\frac{2\hbar\omega_j}{c\epsilon_0 A_j}}e^{i(k_jz-\omega_jt)}\hat{a}_j(\omega_j), \tag{3}$$

where A_j, k_j, and $\hat{a}_j(\omega_j)$ denote the (continuous-mode) cross-section areas, wave vectors, and annihilation operators, respectively, with $j \in \{s, as, as'\}$ [47]. We will take $A_s = A_{as} = A_{as'}$ for simplicity and use a common area A_c to represent them in the following discussions.

Explicit expressions for the *linear* $\chi_j^{(1)}$ and *nonlinear* $\chi_{i,j}^{(3)}$ susceptibilities in Eqs. (2) are rather involved and can be found in the Appendix. In the following we just focus on the *linear* susceptibilities, while leaving the *nonlinear* susceptibilities responsible for SFWM processes to the next section. The linear susceptibility in P_{52}, for instance, consists of two terms,

$$\chi_s^{(1)} = \chi_S^{(1)} + \tilde{\chi}_S^{(1)}. \tag{4a}$$

The first term $\chi_S^{(1)}$ is proportional to the population difference $\rho_{22}^{\langle 0\rangle} - \rho_{55}^{\langle 0\rangle}$ and takes the form of an EIT susceptibility for the V subsystem of three levels $\{|5\rangle, |2\rangle, |4\rangle\}$ (see Appendix). To assess loss (gain) exhibited by Stokes photons we introduce the (real) figure of merit,

$$\eta_S = 1 - \exp\big[-\mathrm{Im}\chi_S^{(1)}\omega_sL/c\big], \tag{4b}$$

being L the sample length. The second term $\tilde{\chi}_S^{(1)}$, proportional to population differences $\rho_{11}^{\langle 0\rangle} - \rho_{55}^{\langle 0\rangle}$, $\rho_{33}^{\langle 0\rangle} - \rho_{55}^{\langle 0\rangle}$, and $\rho_{22}^{\langle 0\rangle} - \rho_{44}^{\langle 0\rangle}$, represents Raman-like contributions for different subsystems of three levels $\{|1\rangle, |5\rangle, |2\rangle\}$, $\{|3\rangle, |5\rangle, |2\rangle\}$, and $\{|4\rangle, |2\rangle, |5\rangle\}$, respectively (see Appendix). The corresponding loss (gain) of Stokes photons can be assessed through a similar figure of merit,

$$\tilde{\eta}_S = 1 - \exp\big[-\mathrm{Im}\tilde{\chi}_S^{(1)}\omega_sL/c\big]. \tag{4c}$$

Similarly, the linear susceptibility associated with the anti-Stokes transition at ω_{as} can be cast as

$$\chi_{as}^{(1)} = \chi_{AS}^{(1)} + \tilde{\chi}_{AS}^{(1)}, \tag{5a}$$

where $\chi_{AS}^{(1)}$ is proportional to $\rho_{11}^{\langle 0\rangle} - \rho_{44}^{\langle 0\rangle}$ and takes the form of an EIT susceptibility for a Λ subsystem of three levels $\{|1\rangle, |4\rangle, |2\rangle\}$. Once again $\tilde{\chi}_{AS}^{(1)}$ represents Raman-like contributions arising from three subterms proportional to $\rho_{11}^{\langle 0\rangle} -$

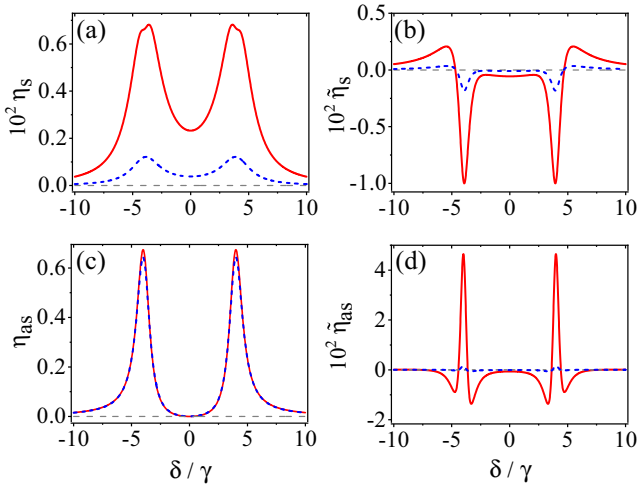

FIG. 3. Linear absorption or gain of the generated Stokes (a),(b) and anti-Stokes (c),(d) fields for process A plotted against the common two-photon detuning δ with $\Omega_p = \Omega_{p'} = \gamma/5$ and $\gamma_0 = 2\pi \times 15$ kHz for red-solid curves while $\Omega_p = \Omega_{p'} = \gamma/25$ and $\gamma_0 = 2\pi \times 3$ kHz for blue-dashed curves. Other parameters are the same as in Fig. 2 except sample length $L = 100$ μm, atomic density $N_0 = 9.0 \times 10^{11}$ cm^{-3}, and dipole moments $\mu_{24,25} = \sqrt{3}\mu_{14,15,34,35} = 1.268 \times 10^{-29}$ Cm.

$\rho_{55}^{\langle 0\rangle}$, $\rho_{33}^{\langle 0\rangle} - \rho_{55}^{\langle 0\rangle}$, and $\rho_{22}^{\langle 0\rangle} - \rho_{44}^{\langle 0\rangle}$, respectively. Accordingly, the two figures of merit,

$$\eta_{AS} = 1 - \exp\big[-\mathrm{Im}\chi_{AS}^{(1)}\omega_{as}L/c\big], \tag{5b}$$

$$\tilde{\eta}_{AS} = 1 - \exp\big[-\mathrm{Im}\tilde{\chi}_{AS}^{(1)}\omega_{as}L/c\big], \tag{5c}$$

can be introduced to assess the loss (gain) of anti-Stokes photons resulted from $\mathrm{Im}\chi_{AS}^{(1)}$ and $\mathrm{Im}\tilde{\chi}_{AS}^{(1)}$, respectively. As for the linear susceptibility $\chi_{as'}^{(1)}$ in P_{43}, it follows directly upon the subscript replacements $as \to as'$, $p \to p'$, and $1 \to 3$ in corresponding expressions.

We plot in Fig. 3 $\eta_{S,AS}$ and $\tilde{\eta}_{S,AS}$ for process A to assess loss (positive) and gain (negative) of the generated Stokes and anti-Stokes fields, which can be largely suppressed even for resonant pumpings as shown below. It is easy to find from Figs. 3(a) and 3(c) that η_S and η_{AS} exhibit two-peaks EIT spectra corresponding to the V and Λ subsystems, respectively. Owing to the formation of a quasidark state, loss is quite small near $\delta = 0$ for η_S because negligible populations exist in the V subsystem, and for η_{AS} because destructive interference occurs in the Λ subsystem. As for $\tilde{\eta}_S$ and $\tilde{\eta}_{AS}$, Figs. 3(b) and 3(d) show that they exhibit typical features of Raman-like gain or loss, which is also small near $\delta = 0$ but becomes important in two regions overlapping with the EIT peaks. This can be understood by rewriting $\chi_S^{(1)}$ and $\chi_{AS}^{(1)}$ as a sum of two (Lorentz) resonance profiles,

$$\chi_S^{(1)} = -iN_0\frac{\mu_{25}^2(\rho_{22}^{\langle 0\rangle} - \rho_{55}^{\langle 0\rangle})(\gamma_{54} + i\delta)}{2\hbar\epsilon_0\Omega_{e1}} \times\left[\frac{1}{(\delta - \Omega_{e1}) - i\gamma_{e1}} - \frac{1}{(\delta + \Omega_{e1}) - i\gamma_{e1}}\right], \tag{6a}$$

$$\chi_{AS}^{(1)} = -iN_0\frac{\mu_{14}^2(\rho_{11}^{\langle 0\rangle} - \rho_{44}^{\langle 0\rangle})(\gamma_{21} - i\delta)}{2\hbar\epsilon_0\Omega_{e2}} \times\left[\frac{1}{(\delta - \Omega_{e2}) + i\gamma_{e2}} - \frac{1}{(\delta + \Omega_{e2}) + i\gamma_{e2}}\right], \tag{6b}$$

in the specific case of $\Delta_c = 0$. Here $\gamma_{e1} = (\gamma_{54} + \gamma_{52})/2$, $\gamma_{e2} = (\gamma_{41} + \gamma_{21})/2$ and $\Omega_{e1} = \sqrt{\Omega_c^2 - (\gamma_{54} - \gamma_{52})^2/4}$, $\Omega_{e2} = \sqrt{\Omega_c^2 - (\gamma_{41} - \gamma_{21})^2/4}$ represent *effective* decoherence rates and Rabi frequencies, respectively.

IV. PHOTON-PAIR GENERATION

The nonlinear spontaneous generation of Stokes and anti-Stokes photon pairs can be described through the effective Hamiltonian $\hat{H}_I = \frac{A_c}{4}\int_0^L dz[\hat{\mathbf{P}}\cdot\hat{\mathbf{E}}^* + \mathrm{H.c.}]$ [22,48], with $\hat{\mathbf{P}} = \hat{P}_{52}\vec{i} + \hat{P}_{41}\vec{j} + \hat{P}_{43}\vec{k}$ and $\hat{\mathbf{E}} = \hat{E}_s^+\vec{i} + \hat{E}_{as}^+\vec{j} + \hat{E}_{as'}^+\vec{k}$ being the overall nonlinear polarization and electric field, respectively. Transferring the linear susceptibilities $\chi_j^{(1)}$ to corresponding wave vectors with $k_j = (1 + \chi_j^{(1)}/2)\omega_j/c$, this Hamiltonian can be further written as

$$\hat{H}_I = \frac{\epsilon_0 A_c}{4}\int_0^L dz\big[\chi_A^{(3)}E_c^+E_p^+\hat{E}_s^-\hat{E}_{as}^- + \chi_B^{(3)}E_c^+E_{p'}^+\hat{E}_s^-\hat{E}_{as'}^- + \chi_{as,as'}^{(3)}E_{p'}^+E_p^-\hat{E}_{as}^+\hat{E}_{as'}^- + \chi_{as',as}^{(3)}E_p^+E_{p'}^-\hat{E}_{as'}^+\hat{E}_{as}^-\big] + \mathrm{H.c.}, \tag{7}$$

describing the wave-mixing processes A, B, and C embedded in Eqs. (2). The first term corresponds to process A responsible for the generation of a photon pair $\{\omega_s, \omega_{as}\}$ with $\chi_A^{(3)} = \chi_{as,s}^{(3)} + \chi_{s,as}^{(3)}$, while the second term corresponds to process B responsible for the generation of a photon pair $\{\omega_s, \omega_{as'}\}$ with $\chi_B^{(3)} = \chi_{as',s}^{(3)} + \chi_{s,as'}^{(3)}$. The last two terms account for process C associated with the interchange of anti-Stokes photons $\{\omega_{as}, \omega_{as'}\}$.

In the quasidark-state regime, for sufficiently weak (resonant) pumpings, nonlinear interactions can be made weak enough to prevent the generation of more than one pair of Stokes and anti-Stokes photons. Thus, the first-order evolution $\hat{\mathbb{I}} + \frac{i}{\hbar}\int dt\,\hat{H}_I$ will project the vacuum [49] onto the state $|\Psi\rangle \simeq |0\rangle + |\Psi\rangle_A + |\Psi\rangle_B + \cdots$, where the component at $\{\omega_s, \omega_{as}\}$ takes the form [34,48]

$$|\Psi\rangle_A = L\int d\delta\,\Phi_A(\delta)\kappa_A(\delta)\hat{a}_s^\dagger(\delta)\hat{a}_{as}^\dagger(\delta)|0_s, 0_{as}, 0_{as'}\rangle, \tag{8}$$

with the consideration of energy conservation ($\omega_s + \omega_{as} = \omega_p + \omega_c$). While a similar expression holds naturally for the other biphoton state $|\Psi\rangle_B$, it is worth noting that process C does not occur when $\delta_s = -\delta_{as}$ is exactly equal to $\delta_{s'} = -\delta_{as'}$ and remains negligible even if $\delta_s = -\delta_{as}$ is slightly different from $\delta_{s'} = -\delta_{as'}$ provided two balanced pumpings ($\Omega_p = \Omega_{p'}$ and $\Delta_p = \Delta_{p'}$) hold, which is the regime of interest in the present work.

The phase mismatch for process A is

$$\Phi_A = \exp\left(-\frac{i\Delta k_A L}{2}\right)\mathrm{sinc}\left(\frac{\Delta k_A L}{2}\right), \tag{9}$$

being $\Delta k_A = k_s^* + k_{as}^* - k_p - k_c$ the complex wave-vector mismatch. Through a standard expansion of the wave vectors k_s, k_{as}, k_p, and k_c in terms of the linear susceptibilities $\chi_s^{(1)}$,

$\chi_{as}^{(1)}$, $\chi_{p}^{(1)}$, and $\chi_{c}^{(1)}$ (see Appendix) and reserving only the dominant ones, we have

$$\frac{\Delta k_A L}{2} \simeq -\frac{\omega_p L}{4c}\chi_p^{(1)} \simeq -i\frac{\pi N_0 L}{4\epsilon_0 \hbar}\frac{\mu_{15}^2}{\lambda_p}\frac{1}{\gamma_{51}+\mathcal{A}_0}, \tag{10a}$$

for values of $\delta = 0$ and far from $\pm\Omega_{e2}$ while

$$\begin{aligned}\frac{\Delta k_A L}{2} &\simeq -\frac{\omega_p L}{4c}\chi_p^{(1)} + \frac{\varpi_{as} L}{4c}\chi_{AS}^{(1)*} \\ &\simeq -i\frac{\pi N_0 L}{4\hbar\epsilon_0}\left[\frac{\mu_{15}^2}{\lambda_p}\frac{1}{\gamma_{51}+\mathcal{A}_0} + \frac{\mu_{14}^2}{\lambda_{as}}\frac{1}{\gamma_{41}}\right],\end{aligned} \tag{10b}$$

when $\delta = \pm\Omega_{e2}$. Here, $\varpi_s = \omega_p - \omega_{21}$ and $\varpi_{as} = \omega_c + \omega_{21}$ are introduced to denote the Stokes and anti-Stokes central frequencies, respectively, both corresponding to $\delta = 0$ due to the requirement of energy conservation $\varpi_s + \varpi_{as} = \omega_p + \omega_c$. This is justified by considering that the Stokes and anti-Stokes photon pairs are generated with an extremely narrow bandwidth centered at $\delta = 0$ so that it is appropriate to take $\omega_{s,as} \to \varpi_{s,as}$ in the wave vectors $k_{s,as} \propto \omega_{s,as}/c$, a replacement that cannot be done in the linear and nonlinear susceptibilities being rapidly varying functions of δ. In addition, we note that

$$\mathcal{A}_0 = \Omega_{p'}^2(\gamma_{51}+\gamma_{53})/\gamma_{31}\gamma_{53} \tag{11}$$

describes the effect of the other pumping needed to generate the quasidark state. Equation (10b) indicates that $|\Phi_A|$ would exhibit two dips at $\delta = \pm\Omega_{e2}$ due to the remarkable loss of anti-Stokes photons (cf. Fig. 3) while Eq. (10a) indicates that $|\Phi_A| \to 1$ could be observed around $\delta = 0$ provided $\mathcal{A}_0$ is much larger than γ_{51}. In deriving Eq. (10a) and (10b), we have also considered that $\chi_s^{(1)}$ (cf. Fig. 3) and $\chi_c^{(1)}$ are negligible because little populations appear in levels $|2\rangle$, $|4\rangle$, and $|5\rangle$.

The wave-mixing function for process A

$$\kappa_A = -i\frac{\sqrt{\varpi_{as}\varpi_s}}{2c}\left[\chi_{as,s}^{(3)}(\delta) + \chi_{s,as}^{(3)}(\delta)\right]E_p^+ E_c^+ \tag{12}$$

has been attained from $\hat{\mathbb{I}} + \frac{i}{\hbar}\int dt\, \hat{H}_I$ by considering that ω_s and ω_{as} are related through $\delta = \delta_s = -\delta_{as}$ for fixed Δ_p and Δ_c. In the case of $\Delta_p = \Delta_c = 0$, the first nonlinear susceptibility takes the form

$$\begin{aligned}\chi_{as,s}^{(3)} =& iN_0\frac{\mu_{25}\mu_{15}\mu_{14}\mu_{24}}{16\hbar^3\epsilon_0}\frac{1}{(\gamma_{51}+\mathcal{A}_0)\Omega_{e2}} \\ &\times\left[\frac{1}{(\delta-\Omega_{e2})+i\gamma_{e2}} - \frac{1}{(\delta+\Omega_{e2})+i\gamma_{e2}}\right],\end{aligned} \tag{13a}$$

which comprises two Lorentz resonances centered at $\pm\Omega_{e2}$ with an identical width γ_{e2} and exhibits a monotonic growth with γ_{31} in the limit of $\mathcal{A}_0 \gg \gamma_{51}$.

The second nonlinear susceptibility in Eq. (12), though derived under the same pumping and coupling conditions for Eq. (24), takes a more involved form

$$\begin{aligned}\chi_{s,as}^{(3)} =& iN_0\frac{\mu_{25}\mu_{15}\mu_{14}\mu_{24}}{16\hbar^3\epsilon_0}\frac{\mathcal{A}_1}{\mathcal{A}_2(\gamma_{51}+\mathcal{A}_0)\Omega_{e3}} \\ &\times\left[\frac{1}{(\delta-\Omega_{e3})-i\gamma_{e3}} - \frac{1}{(\delta+\Omega_{e3})-i\gamma_{e3}}\right],\end{aligned} \tag{13b}$$

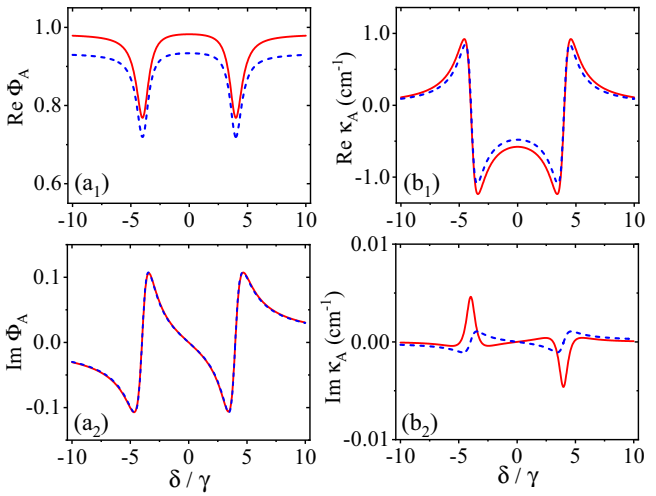

FIG. 4. Real (a_1) and imaginary (a_2) parts of the phase mismatch Φ_A as well as real (b_1) and imaginary (b_2) parts of the wave-mixing function κ_A for process A plotted against the common two-photon detuning δ. Relevant parameters are the same as in Fig. 3 except $\Omega_p = \Omega_{p'} = \gamma/5$ and $\gamma_0 = 2\pi \times 15$ kHz refer to red-solid curves while $\Omega_p = \Omega_{p'} = \gamma/25$ and $\gamma_0 = 2\pi \times 3$ kHz refer to blue-dashed curves.

where $\mathcal{A}_1 = \Omega_c^2 + \gamma_{51}\gamma_{54} - \delta^2 + i\delta(\gamma_{43}+2\gamma_{51})$, $\mathcal{A}_2 = \Omega_c^2 + \gamma_{52}\gamma_{54} - \delta^2 + i\delta(\gamma_{52}+\gamma_{54})$, $\gamma_{e3} = (\gamma_{43}+\gamma_{32})/2$, and $\Omega_{e3} = \sqrt{\Omega_c^2 - (\gamma_{43}-\gamma_{32})^2/4}$. For the choice of atomic levels considered in our numerical calculations, we have $\gamma_{21} = \gamma_{32} \ll \gamma_{41} = \gamma_{43} = \gamma_{51} = \gamma_{52} = \gamma_{54}/2$, hence $\Omega_{e1} \simeq \Omega_{e2} = \Omega_{e3}$, $\gamma_{e1} \simeq 3\gamma_{e2} = 3\gamma_{e3}$, and $\mathcal{A}_1 = \mathcal{A}_2$. In this case, we have $\chi_{as,s}^{(3)*} \simeq -\chi_{s,as}^{(3)}$ so that to a good approximation κ_A becomes real and equal to

$$\kappa_A = \frac{\sqrt{\varpi_{as}\varpi_s}}{c}\,\mathrm{Im}\left[\chi_{as,s}^{(3)}(\delta)\right]E_p^+ E_c^+, \tag{14}$$

which is proportional to γ_{31}/Ω_p in the limit of $\mathcal{A}_0 \gg \gamma_{51}$. This conclusion holds also for the wave-mixing function κ_B (process B) where $\chi_{as',s}^{(3)}$ and $\chi_{s,as'}^{(3)}$ should be considered instead. Hence, the SFWM efficiencies for processes A and B are determined only by imaginary parts of relevant third-order susceptibilities.

Then we plot in Fig. 4 real and imaginary parts of Φ_A as well as real and imaginary parts of κ_A to seek a spectral region where efficient SFWM processes could be observed for two balanced pumping fields. It is clear that a very good phase matching with $\mathrm{Re}\Phi_A \to 1$ and $\mathrm{Im}\Phi_A \to 0$ has been found everywhere except around two resonant points determined by $\delta = \pm\Omega_{e2} = \pm\Omega_{e3}$. A very strong third-order nonlinearity with $\mathrm{Re}[\kappa_A] \simeq -0.5\ \mathrm{cm}^{-1}$ and $\mathrm{Im}[\kappa_A] \to 0$ exists, however, in a small region centered at $\delta = 0$ including the two resonant points. So efficient SFWM processes occur only between the two resonant points, where a good phase matching and a strong third-order nonlinearity are associated with weak linear absorption and gain (cf. Fig. 3). These numerical findings are well supported by relevant approximate equations, which show that $\mathrm{Re}\Phi_A$ will be evidently improved while $\mathrm{Re}\kappa_A$ will remain roughly unchanged as $\Omega_{p'}/\gamma_{31}$ is increased to result in $\mathcal{A}_0 \gg \gamma_{51}$.

Next we consider the intensity correlation function of a Stokes photon ω_s at time t_s while an anti-Stokes photon ω_{as} at time t_{as} generated in process A:

$$G_A^{(2)}(t_s, t_{as}) = |\langle 0|\hat{a}_s(t_s)\hat{a}_{as}(t_{as})|\Psi\rangle_A|^2. \tag{15}$$

This function, after including $|\Psi\rangle_A$ in Eq. (8) and

$$\hat{a}_j(t_j) = \frac{1}{\sqrt{2\pi}} \int d\omega_j \hat{a}_j(\omega_j) e^{i(k_j L - \omega_j t_j)}, \tag{16}$$

turns out to be

$$G_A^{(2)}(\tau) = \frac{L^2}{4\pi^2} \left| \int d\delta\, \kappa_A(\delta)\Phi_A(\delta) e^{i(k_s + k_{as})L} e^{-i\delta\tau} \right|^2, \tag{17a}$$

proportional to the modulus square of a Fourier transformation on the product $\kappa_A\Phi_A$ with $\tau = t_{as} - t_s$. The Stokes wave vector k_s can be treated, to a good approximation, as a constant ϖ_s/c since $|\chi_s^{(1)}|$ is much smaller than unity, which is clear from Figs. 3(a) and 3(b). The anti-Stokes wave vector k_{as} should be seen, however, as a sum of ϖ_{as}/c and δ/v_g, being v_g the group velocity much smaller than the vacuum light speed c. This is based on the fact that $\chi_{AS}^{(1)}$ exhibits a strong *normal* dispersion around $\delta = 0$ because η_{AS} is close to unity at $\delta = \pm\Omega_{e2}$ as shown by Fig. 3(c). Benefiting from the concise expression of $\mathrm{Im}\chi_{as,s}^{(3)}$ with two Lorentz resonances, we can use the residue theorem to further attain

$$G_A^{(2)}(\tau) \simeq \frac{\alpha^2\Omega_p^2\Omega_c^2}{\Omega_{e2}^2(\gamma_{51} + \mathcal{A}_0)^2} \exp(-2\gamma_{e2}\tau') \sin^2(\Omega_{e2}\tau'), \tag{17b}$$

which predicts a damped oscillating behavior in the case of $\Omega_{e2} > \gamma_{e2}$ with $\tau' = \tau - L/v_g$ and

$$\alpha = N_0 L |\Phi_{A0}| \frac{\mu_{25}\mu_{14}}{4\hbar\epsilon_0 c} \sqrt{\varpi_{as}\varpi_s}. \tag{18}$$

Here we have considered that $\Phi_A(\delta) \simeq \Phi_A(0) = \Phi_{A0}$ by neglecting the two dips at $\delta = \pm\Omega_{e2}$.

The generation *rate* of biphotons $\{\omega_s, \omega_{as}\}$ can be computed via an integration of $G_A^{(2)}$ over τ as

$$S_A = \int d\tau\, G_A^{(2)}(\tau) \simeq \frac{\alpha^2\Omega_p^2\Omega_c^2}{2\gamma_{e2}\left(\gamma_{e2}^2 + \Omega_{e2}^2\right)(\gamma_{51} + \mathcal{A}_0)^2}, \tag{19}$$

where Eq. (17b) has been taken into account. In Fig. 5(a) we examine the dependence of biphoton generation rate S_A on coupling Rabi frequency Ω_c for two cases of different pumpings (Ω_p) and ground-level dephasings (γ_0). While it gradually increases and saturates at $\Omega_c \gtrsim 0.2\gamma$ for a weaker pumping and dephasing, S_A exhibits instead a fairly rapid growth before decaying from the maximum at $\Omega_c \simeq 0.12\gamma$ to the saturation regime corresponding to $\Omega_c \gtrsim 2\gamma$ for a stronger pumping and dephasing. In both cases, S_A exceeds 10^3 s^{-1} in the saturation regime though it is lower for a weaker pumping and dephasing, which can be understood by taking relevant parameters into $S_A \propto \Omega_p^2/(\gamma_{51} + \mathcal{A}_0)^2 = \gamma_0^2\Omega_p^2/(\gamma_0\gamma + 2\Omega_p^2)^2$.

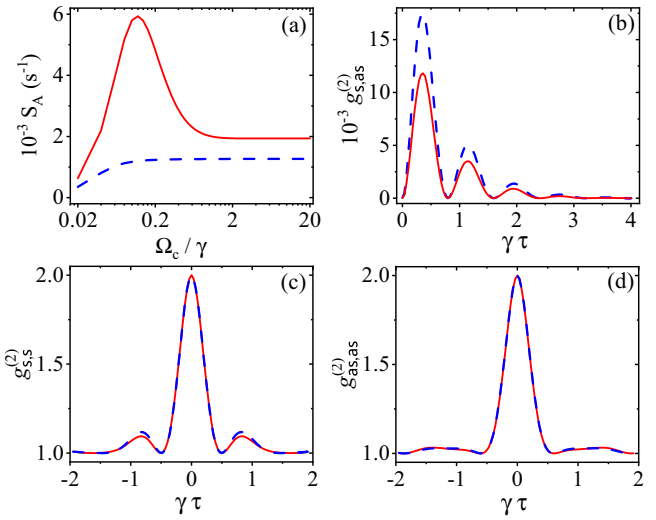

FIG. 5. (a) Biphoton generation rate plotted against the coupling Rabi frequency Ω_c as well as normalized cross- (b) and auto- (c,d) correlation functions plotted against the time delay τ with $\Omega_c = 4\gamma$ for process A. Relevant parameters are the same as in Fig. 3 except $\Omega_p = \Omega_{p'} = \gamma/5$ and $\gamma_0 = 2\pi \times 15$ kHz refer to red-solid curves while $\Omega_p = \Omega_{p'} = \gamma/25$ and $\gamma_0 = 2\pi \times 3$ kHz refer to blue-dashed curves.

We can also calculate the individual generation rates of the Stokes and anti-Stokes photons through

$$R_s = {}_A\langle\Psi|\hat{a}_s^\dagger(t_s)\hat{a}_s(t_s)|\Psi\rangle_A = \frac{L^2}{2\pi}\int d\delta\, f_s(\delta)|\kappa_A(\delta)\Phi_A(\delta)|^2, \tag{20a}$$

$$R_{as} = {}_A\langle\Psi|\hat{a}_{as}^\dagger(t_{as})\hat{a}_{as}(t_{as})|\Psi\rangle_A = \frac{L^2}{2\pi}\int d\delta\, f_{as}(\delta)|\kappa_A(\delta)\Phi_A(\delta)|^2, \tag{20b}$$

with $f_{s,as} = e^{-\mathrm{Im}\chi_{s,as}^{(1)}(\delta)\varpi_{s,as}L/c}$. Their product R_sR_{as} accounts for the accidental coincidence of uncorrelated photons due to the fact that all photon pairs are generated stochastically and different photon pairs exhibit unpredictable time separations [22,23]. Then, it is viable to examine the normalized cross-correlation function

$$g_{s,as}^{(2)}(\tau) = \frac{G_A^{(2)}(\tau)}{R_sR_{as}}, \tag{21}$$

and the normalized autocorrelation functions

$$g_{s,s}^{(2)}(\tau) = \frac{{}_A\langle\Psi^{(2)}|\hat{a}_s^\dagger(0)\hat{a}_s^\dagger(\tau)\hat{a}_s(\tau)\hat{a}_s(0)|\Psi^{(2)}\rangle_A}{R_s^2} = \frac{\left|\frac{L^2}{2\pi}\int d\delta\, f_s(\delta)|\kappa_A(\delta)\Phi_A(\delta)|^2 e^{-i\delta\tau}\right|^2}{R_s^2} + 1, \tag{22a}$$

$$g_{as,as}^{(2)}(\tau) = \frac{{}_A\langle\Psi^{(2)}|\hat{a}_{as}^\dagger(0)\hat{a}_{as}^\dagger(\tau)\hat{a}_{as}(\tau)\hat{a}_{as}(0)|\Psi^{(2)}\rangle_A}{R_{as}^2} = \frac{\left|\frac{L^2}{2\pi}\int d\delta\, f_{as}(\delta)|\kappa_A(\delta)\Phi_A(\delta)|^2 e^{-i\delta\tau}\right|^2}{R_{as}^2} + 1, \tag{22b}$$

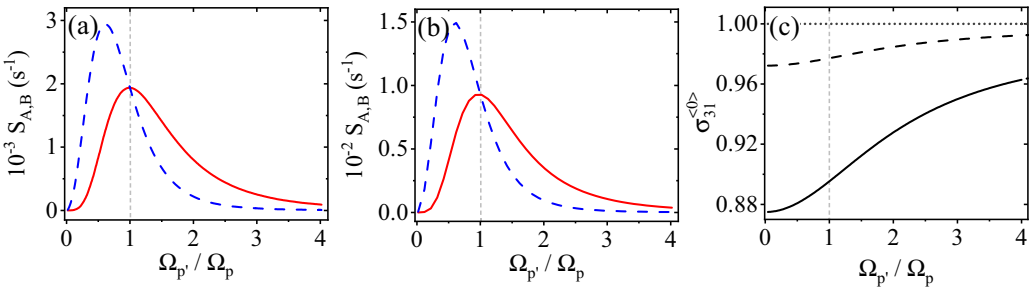

FIG. 6. (a) Biphoton generation rates for processes A (red-solid curve) and B (blue-dashed curve) plotted against the ratio of pumping Rabi frequencies $\Omega_{p'}/\Omega_p$ with $\gamma_0 = 2\pi \times 15$ kHz. (b) Same as above yet with $\gamma_0 = 2\pi \times 3$ kHz. (c) Rescaled ground-level coherence plotted against the ratio of pumping Rabi frequencies $\Omega_{p'}/\Omega_p$ with $\gamma_0 = 0$ (black-dotted line), $\gamma_0 = 2\pi \times 3$ kHz (black-dashed curve), and $\gamma_0 = 2\pi \times 15$ kHz (black-solid curve), respectively. Relevant parameters are the same as in Fig. 3 except $\Omega_p = \gamma/5$.

where $|\Psi^{(2)}\rangle_A = |\Psi\rangle_A|0_s, 0_{as}\rangle + |\Psi\rangle_A|\Psi\rangle_A$ has been considered to include also the event that two pairs of Stokes and anti-Stokes photons are generated with a time delay τ. It is well known that classical light obeys the Cauchy-Schwarz inequality $[g^{(2)}_{s,as}(\tau)]^2/[g^{(2)}_{s,s}(0)g^{(2)}_{as,as}(0)] \leqslant 1$ [22,50]. Hence, the nonclassical property of Stokes and anti-Stokes biphotons can be measured by the extent to which the Cauchy-Schwarz inequality is violated.

As a function of τ in Fig. 5(b), the normalized cross-correlation function $g^{(2)}_{s,as}$ is found to decay at the rate $2\gamma_{e2}$ and oscillate with the period π/Ω_{e2} due to the interference effect arising from the two Lorentz resonances in Eq. (13a). The damped oscillation of $g^{(2)}_{s,as}$ has an inverse dependence on Ω_p and γ_0 as compared to S_A, hence looks higher for a weaker pumping and dephasing. It is also clear that $g^{(2)}_{s,as} \to 0$ at $\tau = 0$, indicating $\tau' \simeq \tau$ in Eq. (17b) with the group delay L/v_g being much smaller than the oscillation period π/Ω_{e2}. We plot in Figs. 5(c) and 5(d) the normalized autocorrelation functions and find that $g^{(2)}_{s,s}(0) = g^{(2)}_{as,as}(0) = 2$, $1 \leqslant g^{(2)}_{s,s}(\tau) \leqslant 2$, and $1 \leqslant g^{(2)}_{as,as}(\tau) \leqslant 2$, reflecting the chaotic nature of Stokes or anti-Stokes photons. The damped oscillations of $g^{(2)}_{s,s}$ and $g^{(2)}_{as,as}$ are seen to be slightly different because we have $f_s \neq f_{as}$ in general though they both approach unity except around $\delta = \pm\Omega_{e2}$. It is more important that the Cauchy-Schwarz inequality is largely violated, namely, by a factor of $\sim 10^7$ with $\max[g^{(2)}_{s,as}]$ being $\sim 1.2 \times 10^4$ or $\sim 1.7 \times 10^4$, thus confirming the strong nonclassical properties of Stokes and anti-Stokes photon pairs.

We further make qualitative discussions on the energy-time entanglement with respect to the biphoton state $|\Psi\rangle_A$. From Eqs. (13a) and (13b) it is easy to see that the Stokes and anti-Stokes photon pairs are generated in process A through two destructively interfering, symmetric Lorentz resonances centered at $\delta = \pm\Omega_{e2}$ (cf. Fig. 4). Considering also the requirement of energy conservation, we know that a Stokes photon generated at the modes $\omega_s^{\pm} = \varpi_s \pm \Omega_{e2}$ must be accompanied by an anti-Stokes photon generated at the modes $\omega_{as}^{\mp} = \varpi_{as} \mp \Omega_{e2}$, suggesting the biphoton entanglement in two pairs of frequency modes with $|\Psi\rangle_A = |\omega_s^+\rangle|\omega_{as}^-\rangle - |\omega_s^-\rangle|\omega_{as}^+\rangle$.

We conclude the section by finally considering the generation rate S_B for process B which is, in general, different from S_A. The two rates are compared in Fig. 6(a) against one pumping ($\Omega_{p'}$) while keeping the other pumping (Ω_p) fixed. Both rates are found to approach zero in the limit of $\Omega_{p'} \ll \Omega_p$ or $\Omega_{p'} \gg \Omega_p$ but exhibit two maxima around $\Omega_{p'}/\Omega_p \simeq 1.0$ and $\Omega_{p'}/\Omega_p \simeq 0.6$, respectively. It is remarkable that, at point $\Omega_{p'}/\Omega_p = 1$, we always achieve the balanced biphoton generation with $S_A = S_B$. The same comparison is carried out in Fig. 6(b) for a different (ground-level) dephasing γ_0. While essentially unchanged in their qualitative features like positions of two maxima and the balanced generation, S_A and S_B exhibit nevertheless an appreciable overall decrease when a smaller γ_0 is used. To be more specific, their balanced values pass from $S_A = S_B > 10^3$ s^{-1} to $S_A = S_B < 10^2$ s^{-1} as γ_0 reduces from $2\pi \times 15$ kHz in Fig. 6(a) to $2\pi \times 3$ kHz in Fig. 6(b). This is associated with an increase of the rescaled ground-level coherence,

$$\sigma_{31}^{\langle 0\rangle} = \frac{|\rho_{31}^{\langle 0\rangle}|}{\sqrt{\rho_{11}^{\langle 0\rangle}\rho_{33}^{\langle 0\rangle}}}. \tag{23}$$

Figure 6(c) shows the expected increase of rescaled coherence $\sigma_{31}^{\langle 0\rangle}$ and hence an decrease of the dark-state dephasing as γ_0 reduces from $2\pi \times 15$ kHz (black-solid line) to $2\pi \times 3$ kHz (black-dashed line). Here we also report, as a reference, the case for an ideal dark state ($\gamma_0 \to 0$), which exhibits no dark-state dephasing and corresponds to a unit value of $\sigma_{31}^{\langle 0\rangle}$ (black-dotted line). Clearly, perturbing an *ideal* dark state into a *quasi*dark state via an increase of γ_0 further leads to larger absorption (gain) of the generated Stokes and anti-Stokes photons, hence γ_0 should be kept much smaller than γ restricted, e.g., by $\gamma_0/\gamma < 0.01$.

V. DOUBLE- VS SINGLE-⋈-SHAPED SYSTEM

Taking $\Omega_{p'} = 0$ and $\Gamma_{53} = \Gamma_{43} = 0$, our double-⋈-shaped system will reduce to the more familiar single-⋈-shaped system used for generating the Stokes and anti-Stokes photon pairs via SFWM. The remaining pumping ($\Omega_p \neq 0$) field is normally far detuned from resonance in order to suppress the linear absorption that may hinder the biphoton generation and avoid other nonlinear interactions that may attenuate the biphoton correlation.

Through a similar calculation, we find that the phase mismatch Φ_A and the wave-mixing function κ_A for process A in our resonant double-⋈-shaped system will become that ($\tilde{\Phi}_A$

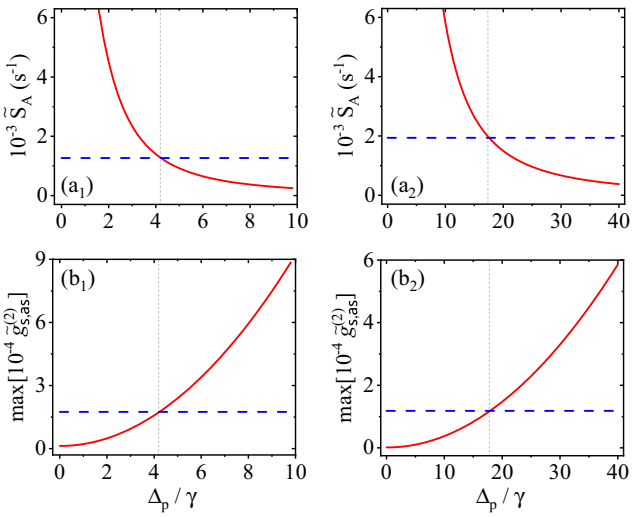

FIG. 7. (a_1),(a_2) Biphoton generation rate and (b_1),(b_2) maximal normalized cross-correlation functions plotted against the pumping detuning Δ_p for a single-$\rhd\lhd$-shaped system. Dashed horizontal lines are corresponding results for a double-$\rhd\lhd$-shaped system with $\Delta_p = 0$. Relevant parameters are the same as in Fig. 3 except $\Omega_p = \Omega_{p'} = \gamma/25$ and $\gamma_0 = 2\pi \times 3$ kHz in (a_1) and (b_1) while $\Omega_p = \Omega_{p'} = \gamma/5$ and $\gamma_0 = 2\pi \times 15$ kHz in (a_2) and (b_2).

and $\tilde{\kappa}_A$) for the off-resonance single-$\rhd\lhd$-shaped system with the simple replacement $\gamma_{51} + \mathcal{A}_0 \to \gamma_{51} + i\Delta_p$. This result seems amazing but is logical because (i) $\mathcal{A}_0$ represents an effective dephasing on transition $|5\rangle \leftrightarrow |1\rangle$ resulted from the other pumping ($\Omega_{p'}$) field as a quasidark state is formed; and (ii) this effective dephasing plays the same role as a large detuning Δ_p in restricting the excitation to level $|5\rangle$ from level $|1\rangle$. Then, it is easy to calculate the biphoton generation rate $\tilde{S}_A$, the normalized cross-correlation function $\tilde{g}^{(2)}_{s,as}$, as well as the normalized autocorrelation functions $\tilde{g}^{(2)}_{s,s}$ and $\tilde{g}^{(2)}_{as,as}$ for the off-resonance single-$\rhd\lhd$-shaped system. We can attain [18,22,48], for instance,

$$\tilde{S}_A = \frac{\alpha^2\Omega_p^2\Omega_c^2}{2\gamma_{e2}\left(\gamma_{e2}^2 + \Omega_{e2}^2\right)|\gamma_{51} + i\Delta_p|^2}, \tag{24}$$

with the same approximations as considered in deriving Eq. (19). A direct comparison shows that $\tilde{S}_A = S_A$ in the case of $(\gamma_{51} + \mathcal{A}_0)^2 = \gamma_{51}^2 + \Delta_p^2$, i.e.,

$$\Omega_{p'}^2 = \frac{\left(\gamma_{51}^2 + \Delta_p^2\right)^{1/2} - \gamma_{51}}{(1 + \gamma_{51}/\gamma_{53})/\gamma_{31}} \simeq \frac{|\Delta_p| - \gamma_{51}}{(1 + \gamma_{51}/\gamma_{53})/\gamma_{31}}, \tag{25}$$

when $|\Delta_p|$ is sufficiently large as compared to γ_{51}. With a further increase of $|\Delta_p|$, our resonant double-$\rhd\lhd$-shaped system will be more efficient, in generating biphotons, than the off-resonance single-$\rhd\lhd$-shaped system. It is expected, however, that a stronger nonclassical cross-correlation will be observed with the increase of $|\Delta_p|$ since $\tilde{g}^{(2)}_{s,as}$ and $\tilde{S}_A$ have an inverse dependence on $\gamma_{51}^2 + \Delta_p^2$, like the inverse dependence of $g^{(2)}_{s,as}$ and S_A on $(\gamma_{51} + \mathcal{A}_0)^2$.

An example of the numerical comparisons is presented in Fig. 7 with the red-solid and blue-dashed lines referring to the single-$\rhd\lhd$-shaped and our double-$\rhd\lhd$-shaped systems, respectively. We find that $\tilde{S}_A$ descends at a lower and lower rate with the increase of Δ_p and becomes inferior to S_A for $\Delta_p \gtrsim 4.2\gamma$ in Fig. 7(a_1) with a weaker pumping and dephasing while for $\Delta_p \gtrsim 17.5\gamma$ in Fig. 7(a_2) with a stronger pumping and dephasing. Figures 7(b_1) and 7(b_2) show that the maximal value of $\tilde{g}^{(2)}_{s,as}$ ascends monotonously with the increase of Δ_p and clearly exceeds the maximal value of $g^{(2)}_{s,as}$ for $\Delta_p \gtrsim 4.2\gamma$ in the case of a weaker pumping and dephasing while for $\Delta_p \gtrsim 17.5\gamma$ in the case of a stronger pumping and dephasing. This means that there exists an inevitable trade-off between the higher generation rate and the stronger nonclassical cross-correlation in regard to generating biphotons via SFWM. Basically, the higher generation rate is more desirable as long as the nonclassical cross-correlation is not too weak with, e.g., $\max[g^{(2)}_{s,as}(\tau)] > 10^3$ and $g^{(2)}_{s,s}(0) = g^{(2)}_{as,as}(0) = 2$. In view of this criterion, our *resonant* double-$\rhd\lhd$ pumping setup is more efficient than the *off-resonance* single-$\rhd\lhd$ pumping setups where typically larger values of Δ_p/γ are used to well reduce the linear absorption or gain while supporting significant SFWM nonlinearities [51–53]. On the other hand, the double-$\rhd\lhd$-shaped and single-$\rhd\lhd$-shaped systems will be not qualitatively different as far as the nonclassical cross-correlation of a biphoton state is concerned.

VI. CONCLUSIONS

In summary, we have investigated an efficient scheme for generating nonclassical biphotons through two partially overlapping *resonant* SFWM processes with identical coupling and Stokes transitions yet different pumping and anti-Stokes transitions. This is achieved by considering a double-$\rhd\lhd$ configuration of atomic levels whereby most populations can be trapped into a quasidark state, largely clear of linear absorption (gain) even if the applied and generated fields are resonant with corresponding transitions. For sufficiently small but nonvanishing ground-level decoherence rates, we can reach an optimal trade-off where nonlinear SFWM is strong enough while linear absorption (gain) is sufficiently weak. The biphoton generation efficiency is comparable to and even larger than that in the more familiar off-resonance single-$\rhd\lhd$ configuration while we can, in addition, exactly balance the two SFWM processes in their generation rates by controlling atomic populations in two ground levels constituting the quasidark state. Our new scheme is viable to be employed, e.g., to herald in an indistinguishable way [34,35] a single photon of either of two colors associated with different anti-Stokes emission channels, and may finally be adapted to solids like Pr^{3+}:Y_2SiO_5 crystals [54–56] where four-wave-mixing effects have been observed.

ACKNOWLEDGMENTS

This work is supported by the National Natural Science Foundation of China (Grants No. 12074061 and No. 11861131001), the Cooperative Program by Italian Ministry of Foreign Affairs and International Cooperation (Grant No. PGR00960), the National Key Research and Development Program of China (Grant No. 2021YFE0193500), and the Scientific and Technological Research Program of Jilin Education Department (Grant No. JJKH20211280KJ).

APPENDIX: LINEAR AND NONLINEAR SUSCEPTIBILITIES

We first define a set of complex decoherence rates with the assumption of $\Delta_p = \Delta_{p'}$:

$$g_{54} = \gamma_{54} + i(\Delta_p + \delta - \Delta_c), \quad g_{53} = \gamma_{53} + i\Delta_{p'}, \quad g_{43} = \gamma_{43} + i(\Delta_c - \delta), \quad g_{32} = \gamma_{32} + i\delta, \quad g_{42} = \gamma_{42} + i\Delta_c,$$
$$g_{52} = \gamma_{52} + i(\Delta_p + \delta), \quad g_{51} = \gamma_{51} + i\Delta_p, \quad g_{41} = \gamma_{41} + i(\Delta_c - \delta), \quad g_{21} = \gamma_{21} - i\delta, \quad g_{31} = \gamma_{31},$$

which are restricted by $g_{ji} = g_{ij}^*$ and will be adopted in the expressions of relevant linear and nonlinear susceptibilities. In the following, we further assume $\Omega_p = \Omega_{p'}$ to consider only two pumping fields of equal strengths since the linear and nonlinear susceptibilities are too complicated in the more general case of $\Omega_p \neq \Omega_{p'}$.

For the applied pumping and coupling fields, their linear susceptibilities can be attained with $R_{ij} = \rho_{ii}^{\langle 0\rangle} - \rho_{jj}^{\langle 0\rangle}$ as

$$\chi_p^{(1)} = \frac{iN_0\mu_{51}^2}{\epsilon_0\hbar}\frac{g_{31}g_{35}R_{15}}{\Omega_p^2 g_{51} + \Omega_{p'}^2 g_{35} + g_{31}g_{35}g_{51}}, \tag{A1a}$$

$$\chi_{p'}^{(1)} = \frac{iN_0\mu_{53}^2}{\epsilon_0\hbar}\frac{g_{13}g_{15}R_{35}}{\Omega_{p'}^2 g_{53} + \Omega_p^2 g_{15} + g_{13}g_{15}g_{53}}, \tag{A1b}$$

$$\chi_c^{(1)} = \frac{iN_0\mu_{42}^2}{\epsilon_0\hbar}\frac{R_{24}}{g_{42}}. \tag{A1c}$$

For the generated Stoke and anti-Stokes fields in process A, their linear susceptibilities have lengthy expressions as a result of the complicated level configuration. In the case of $\Omega_{p,p'} \lesssim 10\sqrt{\gamma_{31}\gamma_{51}}$, however, they become compact and comprise two parts as shown by Eqs. (4a) and (5a) in the main text. One part is simply given by

$$\chi_S^{(1)} = \frac{N_0\mu_{25}^2}{\hbar\epsilon_0}\frac{iR_{25}g_{54}}{\Omega_c^2 + g_{52}g_{54}}, \tag{A2a}$$

$$\chi_{AS}^{(1)} = \frac{N_0\mu_{14}^2}{\hbar\epsilon_0}\frac{iR_{14}g_{21}}{\Omega_c^2 + g_{21}g_{41}}, \tag{A2b}$$

to answer for the EIT-like interactions. The other part further contains three contributions as given by

$$\widetilde{\chi}_S^{(1)} = \chi_{R1}^{(3)}E_p^+E_p^- + \chi_{R2}^{(3)}E_{p'}^+E_{p'}^- + \chi_{R3}^{(3)}E_c^+E_c^-, \tag{A3a}$$

$$\widetilde{\chi}_{AS}^{(1)} = \chi_{R4}^{(3)}E_p^+E_p^- + \chi_{R5}^{(3)}E_{p'}^+E_{p'}^- + \chi_{R6}^{(3)}E_c^+E_c^-, \tag{A3b}$$

to answer for the Raman-like interactions, being $\chi_{Rj}^{(3)}$ relevant nonlinear coefficients.

These nonlinear coefficients are still lengthy. But after introducing $\mathcal{F}_{p'}(x,y) = (x+y)\Omega_{p'}^2 + yg_{31}g_{51}$ and $\mathcal{F}_p(x,y) = (x+y)\Omega_p^2 + yg_{31}g_{53}$ as well as $\mathcal{C}_{p'} = \mathcal{F}_{p'}(g_{51}, g_{35})$ and $\mathcal{C}_p = \mathcal{F}_p(g_{53}, g_{15})$, they can be written as

$$\chi_{R1}^{(3)} = iR_{15}\frac{N_0\mu_{25}^2\mu_{15}^2}{4\hbar^3\epsilon_0} \times \frac{\Omega_c^4\mathcal{F}_{p'}(-\mathcal{C}_{p'}, \mathcal{C}_p) + \Omega_c^2[g_{54}\mathcal{F}_{p'}(\mathcal{C}_{p'}g_{34}, \mathcal{C}_{p'}^*g_{14}) + \mathcal{F}_{p'}(-\mathcal{C}_{p'}g_{12}g_{14}, \mathcal{C}_pg_{32}g_{34})] + g_{14}g_{34}g_{54}\mathcal{F}_{p'}(\mathcal{C}_{p'}g_{12}, -\mathcal{C}_pg_{32})}{\mathcal{C}_p\mathcal{C}_{p'}(\Omega_c^2 + g_{12}g_{14})(\Omega_c^2 + g_{32}g_{34})(\Omega_c^2 + g_{52}g_{54})}, \tag{A4a}$$

$$\chi_{R2}^{(3)} = iR_{35}\frac{N_0\mu_{25}^2\mu_{35}^2}{4\hbar^3\epsilon_0} \times \frac{\Omega_c^4\mathcal{F}_p(-\mathcal{C}_{p'}^*, \mathcal{C}_{p'}) + \Omega_c^2[g_{54}\mathcal{F}_p(\mathcal{C}_{p'}^*g_{14}, -\mathcal{C}_{p'}g_{34}) + \mathcal{F}_p(-\mathcal{C}_pg_{32}g_{34}, \mathcal{C}_{p'}g_{12}g_{14})] - g_{14}g_{34}g_{54}\mathcal{F}_c(-\mathcal{C}_{p'}^*g_{32}, \mathcal{C}_p^*g_{12})}{\mathcal{C}_p\mathcal{C}_{p'}(\Omega_c^2 + g_{12}g_{14})(\Omega_c^2 + g_{32}g_{34})(\Omega_c^2 + g_{52}g_{54})}, \tag{A4b}$$

$$\chi_{R3}^{(3)} = -iR_{24}\frac{N_0\mu_{25}^2\mu_{24}^2}{4\hbar^3\epsilon_0}\frac{1}{g_{24}(\Omega_c^2 + g_{52}g_{54})}, \tag{A4c}$$

$$\chi_{R4}^{(3)} = -iR_{15}\frac{N_0\mu_{14}^2\mu_{15}^2}{4\hbar^3\epsilon_0}\frac{[g_{21}\mathcal{F}_p(g_{53}, g_{25}) - g_{23}\mathcal{F}_p(-g_{53}, g_{43})]\Omega_c^2 + g_{21}g_{23}g_{25}\mathcal{F}_p(-g_{53}, g_{43})}{\mathcal{C}_p(\Omega_c^2 + g_{21}g_{41})(\Omega_c^2 + g_{23}g_{43})(\Omega_c^2 + g_{25}g_{45})}, \tag{A4d}$$

$$\chi_{R5}^{(3)} = -iR_{35}\frac{N_0\mu_{14}^2\mu_{35}^2}{4\hbar^3\epsilon_0}\frac{\Omega_c^4\Omega_p^2 + [g_{23}g_{43} + g_{15}(g_{23} + g_{45})]\Omega_c^2\Omega_p^2 - g_{21}g_{23}g_{25}(g_{15} + g_{43})\Omega_p^2}{\mathcal{C}_p(\Omega_c^2 + g_{21}g_{41})(\Omega_c^2 + g_{23}g_{43})(\Omega_c^2 + g_{25}g_{45})}, \tag{A4e}$$

$$\chi_{R6}^{(3)} = -iR_{24}\frac{N_0\mu_{14}^2\mu_{24}^2}{4\hbar^3\epsilon_0}\frac{1}{g_{24}(\Omega_c^2 + g_{21}g_{41})}. \tag{A4f}$$

Finally, nonlinear susceptibilities for the generated Stokes and anti-Stokes fields in process A are given by

$$\chi^{(3)}_{as,s} = iR_{35}\frac{N_0\mu_{25}\mu_{15}\mu_{14}\mu_{24}}{4\hbar^3\epsilon_0}\frac{\Omega^2_{p'}}{\mathcal{C}_{p'}\left(\Omega_c^2+g_{21}g_{41}\right)} - iR_{15}\frac{N_0\mu_{25}\mu_{15}\mu_{14}\mu_{24}}{4\hbar^3\epsilon_0}\frac{\Omega^2_{p'}+g_{31}g_{35}}{\mathcal{C}_{p'}\left(\Omega_c^2+g_{21}g_{41}\right)}, \tag{A5a}$$

$$\begin{aligned}\chi^{(3)}_{s,as} = &-iR_{15}\frac{N_0\mu_{25}\mu_{15}\mu_{14}\mu_{24}}{4\hbar^3\epsilon_0}\frac{\left(\Omega_c^2+g_{32}g_{34}\right)\left(\Omega^2_{p'}+g_{31}g_{35}\right)-g_{35}(g_{54}+g_{32})\Omega^2_{p'}}{\mathcal{C}_{p'}\left(\Omega_c^2+g_{32}g_{34}\right)\left(\Omega_c^2+g_{52}g_{54}\right)}\\ &+iR_{35}\frac{N_0\mu_{25}\mu_{15}\mu_{14}\mu_{24}}{4\hbar^3\epsilon_0}\frac{\left(\Omega_c^2+g_{32}g_{34}\right)\Omega^2_{p'}+g_{51}(g_{54}+g_{32})\Omega^2_{p'}}{\mathcal{C}_{p'}\left(\Omega_c^2+g_{32}g_{34}\right)\left(\Omega_c^2+g_{52}g_{54}\right)}\\ &-iR_{14}\frac{N_0\mu_{25}\mu_{15}\mu_{14}\mu_{24}}{4\hbar^3\epsilon_0}\frac{g_{12}+g_{54}}{\left(\Omega_c^2+g_{12}g_{14}\right)\left(\Omega_c^2+g_{52}g_{54}\right)}.\end{aligned} \tag{A5b}$$

All linear and nonlinear susceptibilities for the generated Stokes and anti-Stokes fields in process B can be attained from the above equations with the subscript replacements $as \to as'$, $p \to p'$, and $1 \to 3$.

[1] L. M. Duan, M. D. Lukin, J. I. Cirac, and P. Zoller, Long-distance quantum communication with atomic ensembles and linear optics, Nature (London) **414**, 413 (2001).

[2] Y. Mei, Y. Zhou, S. Zhang, J. Li, K. Liao, H. Yan, S.-L. Zhu, and S. Du, Einstein-Podolsky-Rosen Energy-Time Entanglement of Narrow-Band Biphotons, Phys. Rev. Lett. **124**, 010509 (2020).

[3] P. G. Kwiat, K. Mattle, H. Weinfurter, A. Zeilinger, A. V. Sergienko, and Y. Shih, New High-Intensity Source of Polarization-Entangled Photon Pairs, Phys. Rev. Lett. **75**, 4337 (1995).

[4] J.-C. Lee, K.-K. Park, T.-M. Zhao, and Y.-H. Kim, Einstein-Podolsky-Rosen Entanglement of Narrow-Band Photons from Cold Atoms, Phys. Rev. Lett. **117**, 250501 (2016).

[5] T.-M. Zhao, Y. S. Ihn, and Y.-H. Kim, Direct Generation of Narrow-Band Hyperentangled Photons, Phys. Rev. Lett. **122**, 123607 (2019).

[6] H. Yan, S. Zhang, J. F. Chen, M. M. T. Loy, G. K. L. Wong, and S. Du, Generation of Narrow-Band Hyperentangled Nondegenerate Paired Photons, Phys. Rev. Lett. **106**, 033601 (2011).

[7] X. Pan, S. Yu, Y. Zhou, K. Zhang, K. Zhang, S. Lv, S. Li, W. Wang, and J. Jing, Orbital-Angular-Momentum Multiplexed Continuous-Variable Entanglement from Four-Wave Mixing in Hot Atomic Vapor, Phys. Rev. Lett. **123**, 070506 (2019).

[8] S. Li, X. Pan, Y. Ren, H. Liu, S. Yu, and J. Jing, Deterministic Generation of Orbital-Angular-Momentum Multiplexed Tripartite Entanglement, Phys. Rev. Lett. **124**, 083605 (2020).

[9] D. Zhang, Y. Zhang, X. Li, D. Zhang, L. Cheng, C. Li, and Y. Zhang, Generation of high-dimensional energy-time-entangled photon pairs, Phys. Rev. A **96**, 053849 (2017).

[10] N. Gisin and R. Thew, Quantum communication, Nat. Photonics **1**, 165 (2007).

[11] T. Walker, K. Miyanishi, R. Ikuta, H. Takahashi, S. V. Kashanian, Y. Tsujimoto, K. Hayasaka, T. Yamamoto, N. Imoto, and M. Keller, Long-Distance Single Photon Transmission from a Trapped Ion via Quantum Frequency Conversion, Phys. Rev. Lett. **120**, 203601 (2018).

[12] N. Gisin, G. Ribordy, W. Tittel, and H. Zbinden, Quantum cryptography, Rev. Mod. Phys. **74**, 145 (2002).

[13] J. L. O'Brien, Optical quantum computing, Science **318**, 1567 (2007).

[14] I. Buluta, S. Ashhab, and F. Nori, Natural and artificial atoms for quantum computation, Rep. Prog. Phys. **74**, 104401 (2011).

[15] D. Bouwmeester, J. Pan K. Mattle, M. Eibl, H. Weinfurter, and A. Zeilinger, Experimental quantum teleportation, Nature (London) **390**, 575 (1997).

[16] R. Ghosh and L. Mandel, Observation of Nonclassical Effects in the Interference of Two Photons, Phys. Rev. Lett. **59**, 1903 (1987).

[17] L. Mandel, Quantum effects in one-photon and two-photon interference, Rev. Mod. Phys. **71**, S274 (1999).

[18] V. Balić, D. A. Braje, P. Kolchin, G. Y. Yin, and S. E. Harris, Generation of Paired Photons with Controllable Waveforms, Phys. Rev. Lett. **94**, 183601 (2005).

[19] C. H. van der Wal, M. D. Eisaman, A. André, R. L. Walsworth, D. F. Phillips, A. S. Zibrov, and M. D. Lukin, Atomic memory for correlated photon states, Science **301**, 196 (2003).

[20] C.-Y. Hsu, Y.-S. Wang, J.-M. Chen, F.-C. Huang, Y.-T. Ke, E. K. Huang, W. Hung, K.-L. Chao, S.-S. Hsiao, Y.-H. Chen, C.-S. Chuu, Y.-C. Chen, Y.-F. Chen, and I. A. Yu, Generation of sub-MHz and spectrally-bright biphotons from hot atomic vapors with a phase mismatch-free scheme, Opt. Express **29**, 4632 (2021).

[21] L. Zhao, X. Guo, C. Liu, Y. Sun, M. M. T. Loy, and S. Du, Photon pairs with coherence time exceeding 1μs, Optica **1**, 84 (2014).

[22] L. Zhao, Y. Su, and S. Du, Narrowband biphoton generation in the group delay regime, Phys. Rev. A **93**, 033815 (2016).

[23] P. Kolchin, Electromagnetically-induced-transparency-based paired photon generation, Phys. Rev. A **75**, 033814 (2007).

[24] C. Shu, P. Chen, T. K. A. Chow, L. Zhu, Y. Xiao, M. M. T. Loy, and S. Du, Subnatural-linewidth biphotons from a Doppler-broadened hot atomic vapour cell, Nat. Commun. **7**, 12783 (2016).

[25] X. Li, D. Zhang, D. Zhang, L. Hao, H. Chen, Z. Wang, and Y. Zhang, Dressing control of biphoton waveform transitions, Phys. Rev. A **97**, 053830 (2018).

[26] T. Jeong and H. S. Moon, Temporal- and spectral-property measurements of narrowband photon pairs from warm double-Λ type atomic ensemble, Opt. Express **28**, 3985 (2020).

[27] C. Wang, C.-H. Lee, and Y.-H. Kim, Generation and characterization of position-momentum entangled photon pairs in a hot atomic gas cell, Opt. Express **27**, 34611 (2019).

[28] R. T. Willis, F. E. Becerra, L. A. Orozco, and S. L. Rolston, Correlated photon pairs generated from a warm atomic ensemble, Phys. Rev. A **82**, 053842 (2010).

[29] B. Srivathsan, G. K. Gulati, B. Chng, G. Maslennikov, D. Matsukevich, and C. Kurtsiefer, Narrow Band Source of Transform-Limited Photon Pairs via Four-Wave Mixing in a Cold Atomic Ensemble, Phys. Rev. Lett. **111**, 123602 (2013).

[30] M. Fleischhauer, A. Imamoglu, and J. P. Marangos, Electromagnetically induced transparency: Optics in coherent media, Rev. Mod. Phys. **77**, 633 (2005).

[31] K. Liao, H. Yan, J. He, S. Du, Z.-M. Zhang, and S.-L. Zhu, Subnatural-Linewidth Polarization-Entangled Photon Pairs with Controllable Temporal Length, Phys. Rev. Lett. **112**, 243602 (2014).

[32] L. Zhu, X. Guo, C. Shu, H. Jeong, and S. Du, Bright narrowband biphoton generation from a hot rubidium atomic vapor cell, Appl. Phys. Lett. **110**, 161101 (2017).

[33] Q. Y. He, Y. Xue, M. Artoni, G. C. La Rocca, J. H. Xu, and J. Y. Gao, Coherently induced stop-bands in resonantly absorbing and inhomogeneously broadened doped crystals, Phys. Rev. B **73**, 195124 (2006).

[34] A. Zavatta, M. Artoni, and G. La Rocca, Engineering of heralded narrowband color-entangled states, Phys. Rev. A **99**, 031802(R) (2019).

[35] X. J. Zhang, J. H. Wu, G. C. La Rocca, and M. Artoni, Efficient generation of heralded narrowband color-entangled states, Opt. Express **28**, 31076 (2020).

[36] F. Renzoni, W. Maichen, L. Windholz, and E. Arimondo, Coherent population trapping with losses observed on the Hanle effect of the D_1 sodium line, Phys. Rev. A **55**, 3710 (1997).

[37] M. O. Scully and M. S. Zubairy, *Quantum Optics* (Cambridge University Press, Cambridge, UK, 1997).

[38] C. Huang, S. Chai, and S.-Y. Lan, Dark-state sideband cooling in an atomic ensemble, Phys. Rev. A **103**, 013305 (2021).

[39] J. Cerrillo, A. Retzker, and M. B. Plenio, Double-path dark-state laser cooling in a three-level system, Phys. Rev. A **98**, 013423 (2018).

[40] Y. Wang, S. Subhankar, P. Bienias, M. Lacki, T.-C. Tsui, M. A. Baranov, A. V. Gorshkov, P. Zoller, J. V. Porto, and S. L. Rolston, Dark State Optical Lattice with a Subwavelength Spatial Structure, Phys. Rev. Lett. **120**, 083601 (2018).

[41] M. Łacki, M. A. Baranov, H. Pichler, and P. Zoller, Nanoscale "Dark State" Optical Potentials for Cold Atoms, Phys. Rev. Lett. **117**, 233001 (2016).

[42] D. Petrosyan, F. Motzoi, M. Saffman, and K. Mølmer, High-fidelity Rydberg quantum gate via a two-atom dark state, Phys. Rev. A **96**, 042306 (2017).

[43] K. Bergmann, H. Theuer, and B. W. Shore, Coherent population transfer among quantum states of atoms and molecules, Rev. Mod. Phys. **70**, 1003 (1998).

[44] J.-H. Wu, C.-L. Cui, N. Ba, Q.-R. Ma, and J.-Y. Gao, Dynamical evolution and analytical solutions for multiple degenerate dark states in the tripod-type atomic system, Phys. Rev. A **75**, 043819 (2007).

[45] H. R. Gray, R. M. Whitley, and C. R. Stroud, Coherent trapping of atomic populations, Opt. Lett. **3**, 218 (1978).

[46] M. Fleischhauer and M. D. Lukin, Dark-State Polaritons in Electromagnetically Induced Transparency, Phys. Rev. Lett. **84**, 5094 (2000).

[47] R. Loudon, *The Quantum Theory of Light* (Oxford University, New York, 2001).

[48] S. Du, J. Wen, and M. H. Rubin, Narrowband biphoton generation near atomic resonance, J. Opt. Soc. Am. B **25**, C98 (2008).

[49] C. Cohen-Tannoudji, J. Dupont-Roc, and G. Grynberg, *Atom-Photon Interactions* (Wiley, New York, 1998).

[50] A. M. Marino, V. Boyer, and P. D. Lett, Violation of the Cauchy-Schwarz Inequality in the Macroscopic Regime, Phys. Rev. Lett. **100**, 233601 (2008).

[51] P. Kolchin, S. Du, C. Belthangady, G. Y. Yin, and S. E. Harris, Generation of Narrow-Bandwidth Paired Photons: Use of a Single Driving Laser, Phys. Rev. Lett. **97**, 113602 (2006).

[52] S. Du, P. Kolchin, C. Belthangady, G. Y. Yin, and S. E. Harris, Subnatural Linewidth Biphotons with Controllable Temporal Length, Phys. Rev. Lett. **100**, 183603 (2008).

[53] It is, on the other hand, meaningless to have larger $\tilde{S}_A$ for smaller Δ_p where significant absorption (gain) occurs.

[54] H.-H. Wang, D.-M. Du, Y.-F. Fan, A.-J. Li, L. Wang, X.-G. Wei, Z.-H. Kang, Y. Jiang, J.-H. Wu, and J.-Y. Gao, Enhanced four-wave mixing by atomic coherence in a Pr^{3+} : Y_2SiO_5 crystal, Appl. Phys. Lett. **93**, 231107 (2008).

[55] C. Li, Z. Jiang, Y. Zhang, Z. Zhang, F. Wen, H. Chen, Y. Zhang, and M. Xiao, Controlled Correlation and Squeezing in Pr^{3+} : Y_2SiO_5 to Yield Correlated Light Beams, Phys. Rev. Applied **7**, 014023 (2017).

[56] H.-H. Wang, J. Wang, Z.-H. Kang, L. Wang, J.-Y. Gao, Y. Chen, and X.-J. Zhang, Transfer of orbital angular momentum of light using electromagnetically induced transparency, Phys. Rev. A **100**, 013822 (2019).